# Solution-Processed Organic Light-Emitting Transistors Incorporating Conjugated Polyelectrolytes

*Jung Hwa Seo, Ebinazar B. Namdas, Andrea Gutacker, Alan J. Heeger,* and Guillermo C. Bazan**

**Improved performance of *p*-type organic light-emitting transistors (OLETs) is demonstrated by introducing a conjugated polyelectrolyte (CPE) layer and symmetric high work function (WF) source and drain metal electrodes. The OLET comprises a tri-layer film consisting of a hole transporting layer, an emissive layer, and a CPE layer as an electron injection layer. The thickness of the CPE layer is critical for achieving good performance and provides an important structural handle for consideration in future optimization studies. We also demonstrate for the first time, good performance solution-processed blue-emitting OLETs. These results further demonstrate the simplification of device fabrication and improved performance afforded by integrating CPE interlayers into organic optoelectronic devices.**

## 1. Introduction

Organic light-emitting transistors (OLETs) are a class of optoelectronic devices that combine in a single structure the electrical switching functionality of a field-effect transistor (FET) and the capability of light generation from an organic light-emitting diode (OLED).[1–5] OLETs have potential applications in simplified pixels of flat panel displays, optical communication devices, and electrically driven organic lasers.[6–12] There have been a number of studies on OLETs fabricated with solution-processed conjugated polymers, vacuum-deposited thin films of small molecules and single crystals. Accordingly, the device performance of OLETs has rapidly improved.[1,13–18]

OLETs based on a polycrystalline tetracene thin films were demonstrated using interdigitated Au source and drain electrodes on a $Si/SiO_2$ substrate.[2] The device showed typical *p*-type unipolar behavior and light emission from tetracene was observed at the edge of the electrode. In these unipolar OLETs, electrons likely tunnel from the drain electrode into the organic layer, resulting in light emission only in the vicinity of the drain electrode.[2,13,18] Ambipolar OLETs have been more recently demonstrated by using conductive polymers as the active channel and nonpolar polymer dielectrics as the buffer layer to prevent electron trapping at the dielectric-semiconductor interface.[19–21] The position of the emission zone was controlled within the channel region by the gate voltage ($V_G$), so that emission quenching by the metal electrode can be suppressed.[22,23]

The light emitting semiconductor and the nature of hole- and electron- injecting electrodes are critical OLET components.[1–23] Although there are a few materials that transport both holes and electrons, it is still difficult to find organic semiconductors with balanced charge carrier transport and efficient light emission.[13,18,19] Efficient injection of both carriers in OLETs has been accomplished by using low and high work function (WF) metals for the source and drain electrodes.[3,5,10,19,22,24,25] However, there has been a problem of contact properties between the organic layer and metal interface, which limits carrier injection. Furthermore, the complexity of evaporating electrodes with different WF is a practical barrier for application of these devices in color displays. In particular, a typical *p*-type OLET has a high electron injection barrier between the organic layer and the drain electrode. Consequently, a variety of strategies have been implemented to lower the electron injection barrier in both OLED and OLET.[26–29]

Conjugated polyelectrolytes (CPEs) are good electron injection/transport materials and are attractive materials for the development of OFETs, OLEDs, organic solar cells (OSCs), and optically amplified biosensor arrays.[30–35] CPEs are characterized by a $\pi$-conjugated backbone with pendant ionic functional groups. Benefits of these materials include visible transparency, solution processability, and the potential that exists for modifying energy levels at the interface due to ion migration and formation of self-assembled dipole layers. However, the proper application of CPEs requires careful management of the thin film properties, i.e., the thicknesses and surface properties of different underlying layers, and intrinsic energy levels of the material components.[31,35,37]

In this study, we present a solution-processed OLET fabrication methodology, based on the use of a CPE layer as an electron injection layer. To demonstrate the versatility of our method, we

A. Gutacker, Prof. A. J. Heeger, Prof. G. C. Bazan
Center for Polymer and Organic Solids
Department of Chemistry & Biochemistry
University of California at Santa Barbara
Santa Barbara, CA 93106, USA
E-mail: ajhe@physics.ucsb.edu; bazan@chem.ucsb.edu
Prof. J. H. Seo
Department of Materials Physics
Dong-A University
Busan 604-714, Republic of Korea
Prof. E. B. Namdas
Department of Physics
University of Queensland
Brisbane Qld 4072, Australia

**DOI: 10.1002/adfm.201100682**

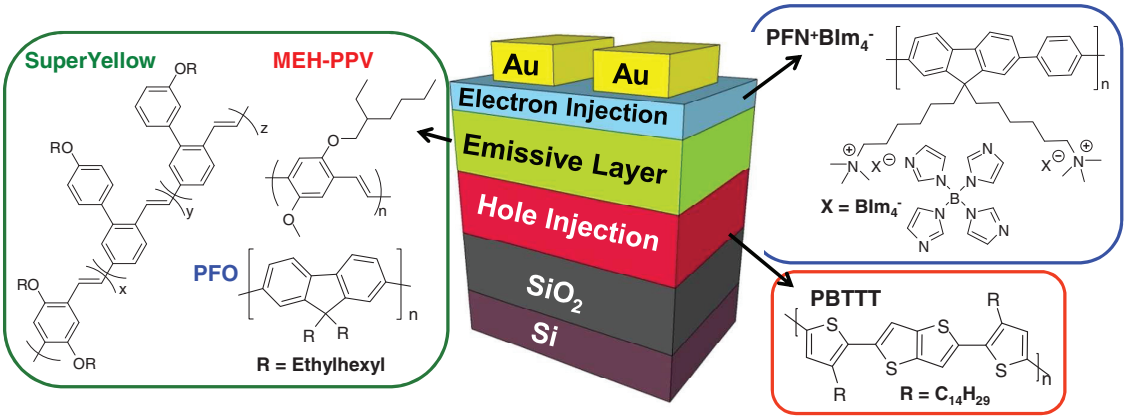


**Scheme 1.** Chemical structures and OLET test device.

fabricated multi-color emission OLETs in which an ultra-thin CPE layer is sandwiched between various emissive layers and source-drain electrodes. The architecture enables the use of high WF charge injection contacts, such as Au, thereby avoiding the air sensitivity resulting from the use of lower WF metal contacts, such as Al, Mg and Ca. The replacement of asymmetric electrodes by symmetric electrodes with a solution-processed CPE layer simplifies fabrication of the display devices, without requiring special procedures for the synthesis of ambipolar organic semiconductors. We believe that these strategies offer a practical alternative for the fabrication of OLETs via low cost techniques.

## 2. Results and Discussion

The basic architecture of the three-component OLET is shown in **Scheme 1**. The channel width ($W$) and length ($L$) were 20 µm and 1000 µm, respectively. Also shown are the corresponding chemical structures used in this study. Poly[9′,9-bis[6′(*N,N,N*-trimethylammonium)hexyl]florene-*alt*-*co*-1,4-phenylene] with tetrakis(imidazoly)borate counterion (**PFN$^+$BIm$_4^-$**) was chosen as an electron injection layer, and poly(2,5-bis(3-alkylthiophene-2-yl)thieno[3,2-b]thiophene) (PBTTT) as a *p*-type semiconductor that is introduced adjacent to the gate dielectric. The emissive layers were selected for various emission colors; a poly[2-methoxy-5-(2′-ethyhexyloxy-1,4-phenylenevinylene)] (MEH-PPV), a phenyl-substituted poly(para-phenylene vinylene) co-polymer (Superyellow; SY) and a poly[9,9-di(ethylhexyl)fluorene] (PFO). To clarify the role of the PBTTT layer, we examined the characteristics of two-component devices with no PBTTT layer (i.e., Au source-drain electrodes deposited atop the CPE layer with MEH-PPV, SY, or PF as the emissive layer). Without PBTTT, the emissive layer must concurrently function as the charge transporting and light emitting material. Devices without the PBTTT layer exhibited no light emission at all negative and positive biases (applied at least for few minutes). Hole current densities generated by two-component devices without the PBTTT layer were always significantly less than the hole current densities of three-component devices. These observations imply that the PBTTT functions as a hole transport material, while MEH-PPV, SY and PFO function as the emissive materials.[10,20,25]

### 2.1. Effect of CPE Thicknesses on OLETs

CPE function was tested within the OLET configuration Si/$SiO_2$/OTS/PBTTT/MEH-PPV/**PFN$^+$BIm$_4^-$**/Au under $N_2$ atmosphere. The concentration of the methanol solution used to deposit the **PFN$^+$BIm$_4^-$** layer was varied. In addition, we fabricated a control device with no CPE layer underneath the Au electrodes. As shown in **Figure 1**a, typical *p*-type transistor

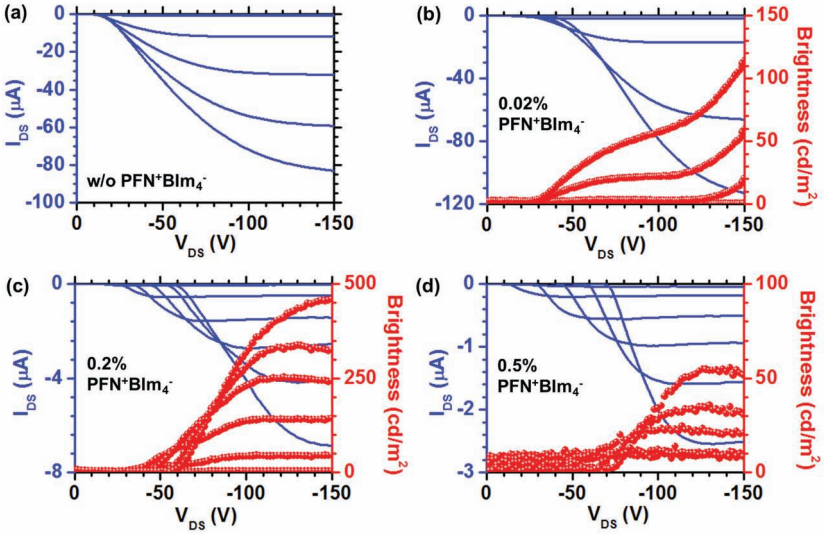


**Figure 1.** a–d) Electrical output (blue line) and optical output (red circle) characteristics of the OLET configuration Si/$SiO_2$/OTS/PBTTT/MEH-PPV/**PFN$^+$BIm$_4^-$**/Au. a) A control device (without CPE layer) is shown for comparison. CPE layers were spin cast from various solutions: b) 0.02%, c) 0.2%, and d) 0.5% on top of the MEH-PPV layer. All devices were annealed at 150 °C for 15 min. ($V_G$ was scanned from 0 to –150 V at intervals of –30 V).

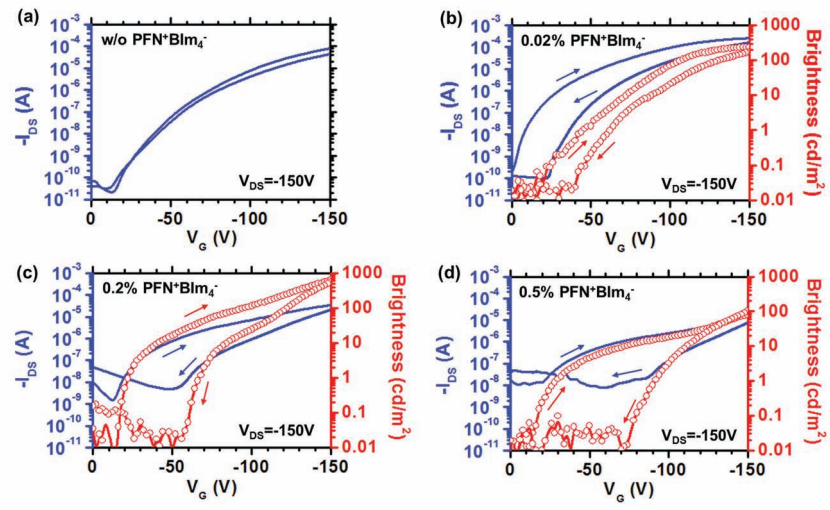


**Figure 2.** a–d) Electrical transfer (blue line) and optical transfer characteristics (red circle) of corresponding samples in Figure 1a–d. ($V_{DS}$ was fixed at –150 V). Arrows show forward and reverse scans.

behavior is seen in the output characteristics. There is no evidence of electron transport across the channel under positive gate bias.[10,25] Figure 1b–d show output characteristics of the OLETs in which **PFN$^+$BIm$_4^-$** layers were deposited from 0.02%, 0.2%, and 0.5% solutions. As shown in Figure 1b, a device fabricated with a dilute **PFN$^+$BIm$_4^-$** solution exhibits typical *p*-type FET characteristics (negatively biased gate electrode) with clear saturation behavior. Examination of the output characteristics of the OLETs with higher loadings, i.e., 0.2% and 0.5% **PFN$^+$BIm$_4^-$** solutions, Figure 1c,d, respectively, reveals unusual saturation behavior due to additional bulk current within the 8 ~ 15 nm **PFN$^+$BIm$_4^-$** layers. The shifting of the source-drain current ($I_{DS}$) with source-drain voltage ($V_{DS}$) in Figure 1c,d is attributed to ion motion within the **PFN$^+$BIm$_4^-$** layer.[31,36–38] In Figure 1b–d, there is a trend of decreasing $I_{DS}$ with the increase of the **PFN$^+$BIm$_4^-$** solution concentration. This lower current arises from (i) the electric field screening due to mobile ions and (ii) a modification of the energy level alignment by the effect on the dipoles.

**Figure 2**a–d show the OLET electrical transfer characteristics. The devices exhibit typical *p*-type transistors with no indication of ambipolar operation. Nor was it possible to operate the transistor in pure *n*-type mode. Based on Figure 1 and 2, the device treated with dilute **PFN$^+$BIm$_4^-$** solutions exhibits excellent *p*-type transistor characteristics with mobility ($\mu$) of ~0.1 cm$^2$/V·s and a current on/off ratio ($I_{on}/I_{off}$) ~ $10^7$. The device performance is comparable to that of the control device with no **PFN$^+$BIm$_4^-$** layer. In addition, the curves in Figure 2b–d show mismatch between forward and reverse scan (hysteresis) that can be assigned to the degree to which $I_{DS}$ depends on the direction of the $V_G$ sweep. A larger hysteresis is observed with increasing the concentration of CPE solutions. Such hysteresis is detrimental to the transistor functions due to charge trapping in deep states, and/or dipole physical rearrangement, mobile ion accumulation.[39]

Figure 1 and 2 (red curves) show the optical output versus $V_{DS}$ at various $V_G$ and the optical transfer characteristics versus $V_G$ at $V_{DS}$ = –150 V. For the control device, light emission was not observed under any bias. In Figure 1b–d, light emission is observed in the saturation regime and is a characteristic of unipolar OLETs. The brightness increases with $V_{DS}$ and $V_G$ then saturates. In Figure 2b–d, the hysteresis of light emission progressively increases and the current on/off ratio decreases; both imply an increase in ion migration. The maximum brightnesses are 112, 639, and 82 cd m$^{-2}$ and the luminescence efficiencies are 0.002, 0.01, and 0.008 (cd/A) for OLETs prepared from solutions of 0.02%, 0.2% and 0.5% **PFN$^+$Bim$_4^-$**, respectively. Electron injection from the CPE/Au electrode is therefore an essential criterion for light emission, although electron transport across the channel is negligible. When the ion-containing layer is sufficiently thin, one can avoid complications associated with electric field redistribution.[31] On the other hand, a proper thickness of the CPE layer results in higher brightness.

### 2.2. Effect of Different Emissive Layers

Whether the CPE could be used for other color emission was tested using OLETs with SY and PFO for yellow-green and blue emissive layers. We examined control devices with no **PFN$^+$BIm$_4^-$** layers underneath the Au electrode. Typical *p*-type transistor behavior was observed for all these device structures at various negative $V_G$ (Supporting Information). No light emission could be measured under these conditions. In order to improve electron injection from high WF electrodes, the solution-processed CPE layers were introduced underneath Au electrodes. **Figure 3** shows the device characteristics of OLETs with **PFN$^+$BIm$_4^-$** layers deposited from 0.02% solutions and different emissive layers. From Figure 3, devices fabricated with a thin **PFN$^+$BIm$_4^-$** layer exhibit the typical *p*-type FET characteristics with clear saturation behavior. Switching the gate potential leads to no current, which indicates that there is no electron current across the channel.

Light emission corresponding to different emissive layers was observed. Magnified optical images of the working devices are shown in **Figure 4**. Light emission is always observed adjacent to the negative biased electrode, which is assigned as the drain electrode. The region of emission highlights the charge carrier recombination zone. In addition, the position is *independent* of the applied voltage.

From Figure 3, OLET characteristics are observed with saturation behavior; analysis of these curves yield an average $\mu$ of ~0.1 cm$^2$/V·s and an average $I_{on}/I_{off}$ ~ $10^7$. **Table 1** provides a summary of relevant device characteristics. These $\mu$ and $I_{on}/I_{off}$ are higher by two times and a factor of ~$10^2$, respectively, than those obtained for the three-component OLETs with asymmetric electrodes (Ag and Ca).[10,25,40] To the best of our knowledge, there are

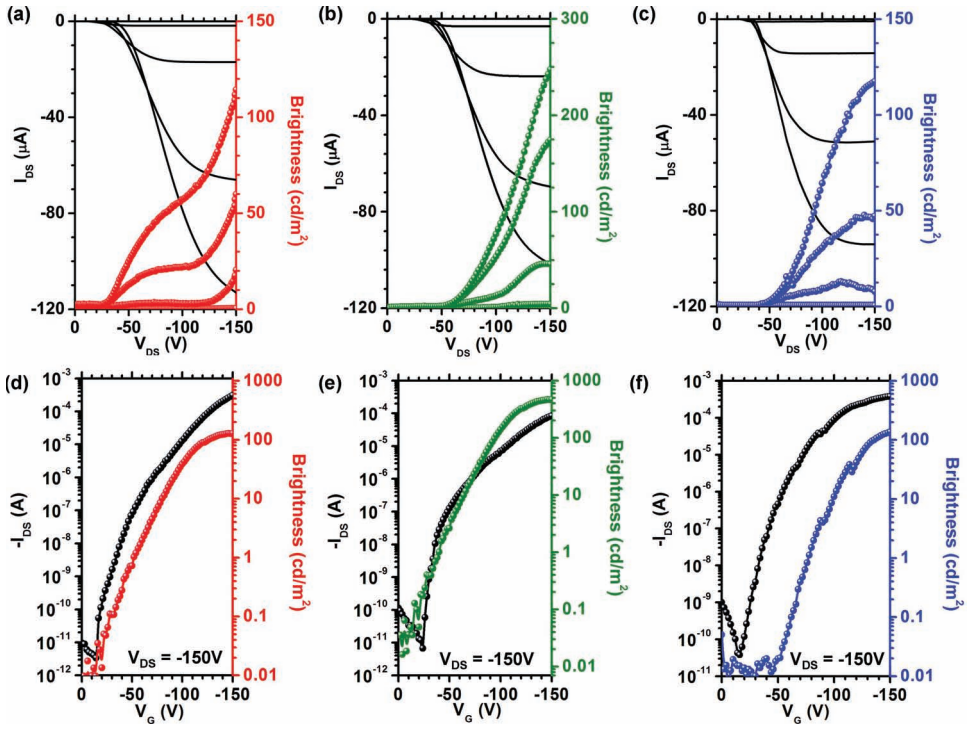


**Figure 3.** a–c) Output and d–f) transfer characteristics of OLETs with: a,d) MEH-PPV, b,e) SY, and c,f) PFO emissive layers. CPE layers were spin cast from 0.02% solution on top of the emissive layer. (In (a–c) $V_G$ was scanned from 0 to –150 V at intervals of –30 V).

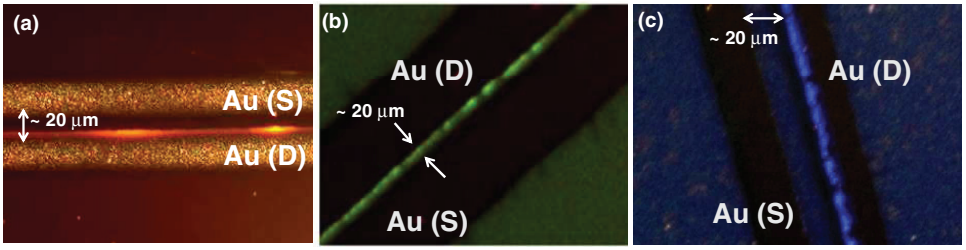


**Figure 4.** Photographs of operating a) orange, b) yellow-green, and c) blue OLETs.

few reports for blue OLETs, but the performance of these devices are relatively low. With using poly[9,9-di(ethylhexyl)-fluorene] emissive layer, we demonstrated here blue OLETs with relatively high transistor performance and luminescence (137 cd m$^{-2}$).

**Table 1.** Summary of charge-transport and light-emitting properties of OLETs.

| | $\mu$ [cm$^2$ V$^{-1}$ s$^{-1}$] | $I_{on}/I_{off}$ | Brightness [cd m$^{-2}$] | $\eta$ [cd A$^{-1}$] | EQE |
|---|---|---|---|---|---|
| Au/MEH-PPV/PBTTT | 0.15 | $10^7$ | - | - | - |
| Au/SY/PBTTT | 0.12 | $10^7$ | - | - | - |
| Au/PFO/PBTTT | 0.14 | $10^7$ | - | - | - |
| Au/PFN$^+$BIm$_4^-$/MEH-PPV/PBTTT | 0.14 | $10^7$ | 112 | 0.002 | $10^{-3}$ |
| Au/PFN$^+$BIm$_4^-$/SY/PBTTT | 0.10 | $10^7$ | 647 | 0.005 | $10^{-3}$ |
| Au/PFN$^+$BIm$_4^-$/PFO/PBTTT | 0.16 | $10^7$ | 137 | 0.004 | $10^{-3}$ |

Typical electroluminescence (EL) spectra for OLETs are displayed in **Figure 5**. Also shown are the corresponding photoluminescence (PL) spectra for MEH-PPV (a), SY (b) and PFO (c). The EL spectra for OLETs with PFO have additional features in the green region of the visible spectrum, centered at approximately 560 nm. The PL and EL spectra of MEH-PPV (Figure 5a) are nearly identical. Since the positions of main peaks of EL spectra are identical to the corresponding PL spectra, the same excitations were involved in both cases. The emission was restricted to the region of the MEH-PPV, SY and PFO layers beneath CPE/Au electrodes. The Commission International de l'Eclairage (CIE) coordinates of the EL emissions are shown in Figure 5d. CIE coordinates were achieved (0.54, 0.44) for MEH-PPV, (0.43, 0.55) for SY and (0.19, 0.24) for PFO at $V_G = V_{DS} = -150$ V.

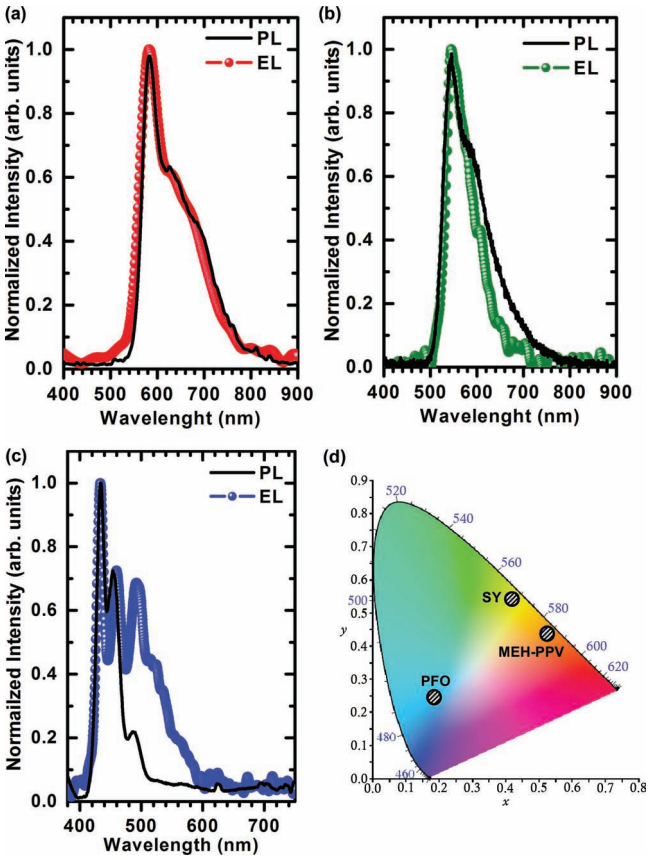


**Figure 5.** EL and PL spectra of OLETs with a) MEH-PPV, b) SY, c) PFO layer, and d) EL CIE coordinates corresponding to (a–c).

### 2.3. Operating Mechanism

We now consider the mechanisms of hole- and electron-charge transport, and light emission in these devices. The energy schematic diagram is shown in **Figure 6**a. Values for the highest occupied molecular orbital (HOMO) and the lowest unoccupied molecular orbital (LUMO) energies of each material were taken from previously published work.[18,19,25] Under negative $V_G$, holes are injected from the Au electrode via the HOMO levels of the emissive layers and transported subsequently across the channel by the PBTTT hole-transporting layer. A key aspect for understanding the device working principle concerns the mechanism of electron injection. With the CPE LUMO energy level at 2.7 eV,[31] electrons have to surmount or tunnel through a barrier of 2.4 eV (from Au). However, the hydrophobic CPE backbone can preferentially interact with the underlying organic layer with the concomitant positioning of the ion component, such that the anions are at the topmost organic surface.[41–43] The use of a thin CPE layer thus leads to the introduction of an interfacial dipole with the positive pole pointing toward the polymer layer and the negative pole toward the metal.[31] Such an orientation raises the effective WF of the Au electrode, as determined by ultraviolet photoelectron spectroscopy (UPS), thereby causing a reduction of the electron injection barrier, (for MEH-PPV, see Supporting Information). Holes are injected at the anode into the HOMO of the PBTTT and transported across the channel.[38] By way of these interfacial charge injection and transport mechanisms, excitons are generated in the emissive layers in the vicinity of the drain electrode and radiatively decay to the ground state.

## 3. Conclusion

A solution-processed fabrication methodology to improve electron injection from the high WF (Au) and to simplify the fabrication of OLETs has been demonstrated. The approach is based upon the use of a CPE layer as an electron injection layer with stable metal electrodes. In this structure, electron injection is enabled by using a thin CPE layer beneath the metal electrode. The thickness of the CPE layer is critical for achieving good performance and provides an important variable for consideration in future optimization studies. The thin CPE layer most likely introduces ordered dipoles at the metal/organic semiconductor interface that facilitate electron injection. Using the CPE layer, we demonstrated multicolor OLET fabrication using different emissive layers. The use of conjugated polyelectrolytes therefore continues to offer new methodologies for the fabrication of devices based upon semiconducting polymers.

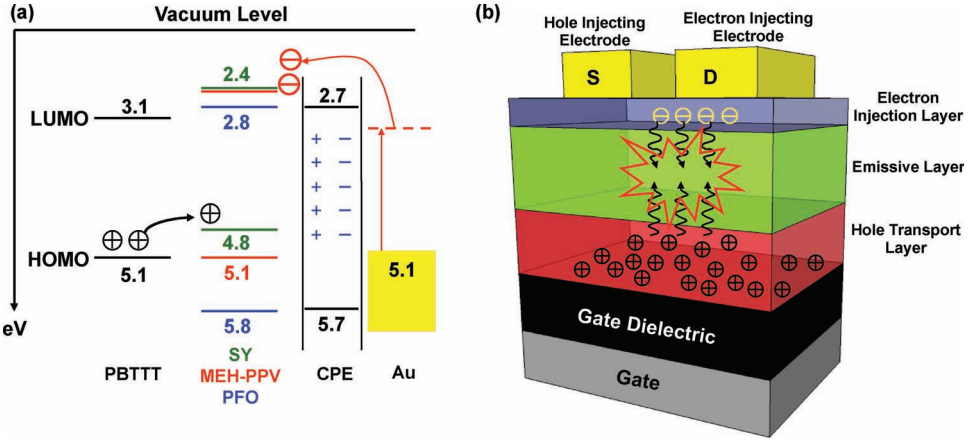


**Figure 6.** a) A proposed energy-level diagram for the three-component OLET device. b) A schematic structure of the OLET on a three component layered architecture reported here.

## 4. Experimental Section

OLETs were fabricated on highly doped *n*-type Si wafers functioned as a substrate and a gate electrode. The octadecyltrichlorosilane (OTS) self-assembled monolayer was formed by immersing the $Si/SiO_2$ substrates in toluene solution for 10 min. PBTTT solution was prepared at 0.3% (w/v) in chlorobenzene. PBTTT films (~65 nm thick) introduced as a hole transporting layer were spin-cast the solution at 3000 rpm for 40 s onto 200 nm $SiO_2$ gate insulator. The films were annealed on a hot plate at 150 °C for 10 min in a $N_2$ glovebox. MEH-PPV, SY, and PFO solutions were prepared at 0.7% (w/v) in toluene and all emissive layers were spin-coated from solutions at 1000 rpm to give film thicknesses of approximately 100 nm. The PBTTT/SY bilayers were annealed at 200 °C for 30 min in a glovebox, while PBTTT/MEH-PPV and PBTTT/PFO bilayers were dried for 20 min in a glovebox without annealing. **$PFN^+Bim_4^-$** films were then deposited by spin-casting from 0.02%, 0.2%, and 0.5% (w/v) solutions in methanol and annealed at 60 °C for 20 min. The 0.2% and 0.5% solutions provided CPE layers on the order of ~8 nm and ~15 nm, respectively, as determined by atomic force microscopy (AFM). While 0.02% solutions of CPEs were too dilute to determine thicknesses. Nonetheless, we have reported that these conditions lead to the deposition atop an organic layer.[31] Finally, 70 nm Au source and drain electrodes were thermally evaporated using a shadow mask. The channel width (*W*) and length (*L*) were 20 μm and 1000 μm, respectively.

The electric and optical measurements were carried out using a Signatone probe station within an $N_2$-atmosphere glovebox. Current-voltage-luminescence characteristics were measured with a Keithley 4200 system and a Hamamatsu photomultiplier (PMT). The photocurrent in the PMT was collected to determine brightness and luminescence efficiency for the effective light emitting area (~$4.0 \pm 0.5$ μm × 1000 μm for all three emissions). This analysis has been described previously in more detail.[40] The EL and PL spectra of the OLETs were acquired using an ocean optics CCD camera with an optical fiber. A digital camera in with an optical microscope was used to visualize light emission of the device.

## Supporting Information

Supporting Information is available from the Wiley Online Library or from the author.

## Acknowledgements

The authors thank the National Science Foundation (DMR-1035480), the Department of Energy (BES, DE-SC0002368) and the Air Force Office of Scientific Research (Charles Lee, Program Officer) for financial support.

Received: March 28, 2011
Published online: July 18, 2011

[1] R. Capelli, S. Toffanin, G. Generali, H. Usta, A. Facchetti, M. Muccini, *Nat. Mater.* **2010**, *9*, 496.
[2] A. Hepp, H. Heil, W. Weise, M. Ahles, R. Schmechel, H. von Seggern, *Phys. Rev. Lett.* **2003**, *91*, 157406.
[3] E. B. Namdas, J. S. Swensen, P. Ledochowitsch, J. D. Yuen, D. Moses, A. J. Heeger, *Adv. Mater.* **2008**, *20*, 1321.
[4] H. Sirringhaus, N. Tessler, R. H. Friend, *Science* **1998**, *280*, 1741.
[5] C. Rost, S. Karg, W. Riess, M. A. Loi, M. Murgia, M. Muccini, *Syn. Metals* **2004**, *146*, 237.
[6] R. Brown, A. Pomp, C. M. Hart, D. M. de Leeuw, *Science* **1995**, *270*, 972.
[7] G. Gelinck, P. Heremans, K. Nomoto, T. D. Anthopoulos, *Adv. Mater.* **2010**, *22*, 3778.
[8] C. Ulbricht, B. Beyer, C. Friebe, A. Winter, U. S. Schubert, *Adv. Mater.* **2009**, *21*, 4418.
[9] M. A. Bader, G. Marowsky, A. Bahtiar, K. Koynov, C. Bubeck, H. Tillmann, H.-H. Hörhold, S. Pereira, *J. Opt. Soc. Am. B* **2002**, *19*, 2250.
[10] E. B. Namdas, M. Tong, P. Ledochowitsch, S. R. Mednick, J. D. Yuen, D. Moses, A. J. Heeger, *Adv. Mater.* **2009**, *21*, 799.
[11] G. Tsiminis, Y. Wang, P. E. Shaw, A. L. Kanibolotsky, I. F. Perepichka, M. D. Dawson, P. J. Skabara, G. A. Turnbull, I. D. W. Samuel, *Appl. Phys. Lett.* **2009**, *94*, 243304.
[12] M. A. Baldo, R. J. Holmes, S. R. Forrest, *Phys. Rev. B* **2002**, *66*, 35321.
[13] M. Muccini, *Nat. Mater.* **2006**, *5*, 605.
[14] F. Cicoira, C. Santato, A. Dadvand, C. Harnagea, A. Pignolet, P. Bellutti, Z. Xiang, F. Rosei, H. Meng, D. F. Perepichka, *J. Mater. Chem.* **2008**, *18*, 158.
[15] T. Takenobu, S. R. Bisri, T. Takahashi, M. Yahiro, C. Adachi, Y. Iwasa, *Phys. Rev. Lett.* **2008**, *100*, 066601.
[16] C. Yumusak, N. S. Sariciftci, *Appl. Phys. Lett.* **2010**, *97*, 033302.
[17] Y. Wang, D. Liu, S. Ikeda, R. Kumashiro, R. Nouch, Y. Xu, H. Shang, Y. Ma, K. Tanigaki, *Appl. Phys. Lett.* **2010**, *97*, 033305.
[18] F. Cicoira, C. Santato, *Adv. Func. Mater.* **2007**, *17*, 3421.
[19] J. Zaumseil, R. H. Friend, H. Sirringhaus, *Nat. Mater.* **2006**, *5*, 69.
[20] J. S. Swensen, C. Soci, A. J. Heeger, *Appl. Phys. Lett.* **2005**, *87*, 253511.
[21] J. S. Swensen, J. Yuen, D. Gargas, S. K. Buratto, A. J. Heeger, *J. Appl. Phys.* **2007**, *102*, 013103.
[22] K. Yamane, H. Yanagi, A. Sawamoto, S. Hotta, *Appl. Phys. Lett.* **2007**, *90*, 162108.
[23] R. C. G. Naber, M. Bird, H. Sirringhaus, *Appl. Phys. Lett.* **2008**, *93*, 023301.
[24] T.-H. Ke, R. Gehlhaar, C.-H. Chen, J.-T. Lin, C.-C. Wu, C. Adachi, *Appl. Phys. Lett.* **2009**, *95*, 063303.
[25] E. B. Namdas, B. B. Y. Hsu, Z. Liu, S.-C. Lo, P. L. Burn, I. D. W. Samuel, *Adv. Mater.* **2009**, *21*, 4957.
[26] H.-H. Chou, C.-H. Cheng, *Adv. Mater.* **2010**, *22*, 2468.
[27] Q. Huang, G. A. Evmenenko, P. Dutta, P. Lee, N. R. Armstrong, T. J. Marks, *J. Am. Chem. Soc.* **2005**, *127*, 10227.
[28] F. Huang, H. Wu, D. Wang, W. Yang, Y. Cao, *Chem. Mater.* **2004**, *16*, 708.
[29] G. Schwartz, S. Reineke, T. C. Rosenow, K. Walzer, K. Leo, *Adv. Func. Mater.* **2009**, *19*, 1319.
[30] M. Sun, L. Lan, L. Wang, J. Peng, Y. Cao, *Macromol. Chem. Phys.* **2008**, *209*, 2504.
[31] J. H. Seo, A. Gutacker, B. Walker, S. Cho, A. Garcia, R. Yang, T.-Q. Nguyen, A. J. Heeger, G. C. Bazan, *J. Am. Chem. Soc.* **2009**, *131*, 18220.
[32] C. V. Hoven, A. Garcia, G. C. Bazan, T.-Q. Nguyen, *Adv. Mater.* **2008**, *20*, 3793.
[33] L. Ding, M. Jonforsen, L. S. Roman, M. R. Andersson, O. Inganäs, *Syn. Metals* **2000**, *110*, 133.
[34] H. Chao, C. Zhong, H. Wu, R. Yang, W. Yang, F. Huang, G. C. Bazan, Y. Cao, *J. Mater. Chem.* **2010**, *20*, 2617.
[35] Y. Wang, B. Liu, A. Mikhailovsky, G. C. Bazan, *Adv. Mater.* **2010**, *22*, 656.
[36] L. Edman, M. Pauchard, B. Liu, D. Moses, A. J. Heeger, *Appl. Phys. Lett.* **2003**, *82*, 3961.
[37] X. L. Chen, Z. Bao, J. H. Schön, A. J. Lovinger, Y.-Y. Lin, B. Crone, A. Dodabalapur, B. Batlogg, *Appl. Phys. Lett.* **2001**, *78*, 228.
[38] J. H. Seo, E. B. Namdas, A. Gutacker, A. J. Heeger, G. C. Bazan, *Appl. Phys. Lett.* **2010**, *97*, 043303.
[39] D. B. A. Rep, A. F. Morpurgo, W. G. Sloof, T. M. Klapwijk, *J. Appl. Phys.* **2003**, *93*, 2082.
[40] E. B. Namdas, P. Ledochowitsch, J. D. Yuen, D. Moses, A. J. Heeger, *Appl. Phys. Lett.* **2008**, *92*, 183304.
[41] H. Li, Y. Xu, C. V. Hoven, C. Li, J. H. Seo, G. C. Bazan, *J. Am. Chem. Soc.* **2009**, *131*, 8903.
[42] L. Lan, J. Peng, M. Sun, J. Zhou, J. Zou, J. Wang, Y. Cao, *Org. Electron.* **2009**, *10*, 346.
[43] J. Park, R. Yang, C. V. Hoven, A. Garcia, D. A. Fischer, T.-Q. Nguyen, G. C. Bazan, D. M. DeLongchamp, *Adv. Mater.* **2008**, *20*, 2491.